Optimal aircraft take-off with thrust vectoring

A.K. Vinayagam
vinayagam@jetmail.ada.gov.in
N.K. Sinha
Department of Aerospace Engineering
Indian Institute of Technology Madras
Chennai, India

ABSTRACT

The short take-off capability is of paramount importance for a fighter airplane to enable its operation from short and damaged runways. This paper analyses the airplane take-off process from the viewpoint of reducing the ground roll/take-off distance with the use of thrust vectoring. The airplane take-off is modelled incorporating the ground reactions on the landing gear and the thrust vector forces and moments. The take-off problem is formulated as an optimal control problem with appropriate constraints. Though many researchers have applied optimal control techniques for designing airplane manoeuvres, its application to the airplane take-off problem is rarely available in the open literature. It is expedient to use such methodology to understand the use of thrust vectoring features of an aircraft to maximise the benefits in shortening the ground roll/take-off distance. An optimal control methodology has been applied in this paper with the objectives stated above to a twin-engine fighter nonlinear aircraft model popularly known as F-18/HARV. Computation of flight path and control schedules using optimal control has been carried out with and without the use of vector nozzles. A reduction of about 6% in take-off distance and about 29% in ground roll distance is obtained with the use of thrust vector for the configuration studied.

Paper No. 3900. Manuscript received 24 August 2012, 1st revised version received 17 April 2013, 2nd revised version received 4 September 2013, accepted 19 September 2013.

https://doi.org/10.1017/S0001924000008733 Published online by Cambridge University Press

NOMENCLATURE

b	wing span (m)
CG	centre of gravity
C_L, C_D, C_m	coefficients of lift, drag and pitching moment, respectively
D	drag (N)
F	force (N)
g	acceleration due to gravity (m/s^2)
L	lift (N)
m	airplane mass (kg)
M	flight Mach number
MAC	mean aerodynamic chord
MLG/NLG	main/nose landing gear
q	body axis pitch rate (rad/s)
R	ground reaction (N)
t	time (s)
TVC	thrust vector control
T_x, T_y, T_z	thrust components in body axes (N)
$\overline{u}$	control vector
V	flight speed (ms^{-1})
$\overline{x}$	state vector
x_{noz}	distance of nozzle deflection axis from CG (m)
x,y,z	body axis co-ordinates
z_{eng}	z-distance between CG and engine axis (m)
α, AoA	angle-of-attack (rad or deg)
δ_e, δ_f, δ_{ptv}	deflection of stabilator, flap & nozzle respectively (deg)
Δx_{mg}, Δz_{mg}	distance from CG to main gear ground contact (m)
Δx_{ng} , Δz_{ng}	distance from CG to nose gear ground contact (m)
η	engine throttle
γ	flight path angle (rad or deg)
μ	coefficient of friction between runway and landing gear
θ	pitch attitude (rad or deg)
θ_R	runway inclination angle (rad or deg)

Subscripts

0	initial value
cg	centre of gravity
f	final value
l	lower limit
mg	main landing gear
ng	nose landing gear
b	body co-ordinate system
E	Earth co-ordinate system
SL	sea level
u	upper limit
x, y, z	body axis components in x, y and z

https://doi.org/10.1017/S0001924000008733 Published online by Cambridge University Press

1.0 INTRODUCTION

Fighter airplane take-off is one of the classic problems in the field of flight mechanics and control. The short take-off capability is of paramount importance for a fighter aircraft to enable its operation from short and damaged runways. Take-off is a complex flight manoeuvre involving different distinct sequential phases of ground run, rotation and lift-off, transition and climb. Use of thrust vectoring in fighter aircraft is believed to help in shortening the take-off distance, but it further complicates the control during take-off. An attempt has been made in this work to understand the optimal control strategy and also the use of thrust vectoring for the take-off. Even though the optimal control technique has been applied to many problems in aircraft flight dynamics, its application to the take-off problem is rarely seen in open literature.

Modern aircraft such as the Su-30, Mig-29 OVT/Mig-35, F-22, F-35, PAK-FA are equipped with thrust vector nozzles and the Eurofighter Typhoon may have thrust vector nozzle in the future[1]. The thrust vector nozzle is mainly used to gain dominance in the close air combat. It provides controllability to the aircraft in the post-stall region where the conventional aerodynamic controls are ineffective[2,3]. Thrust vectoring can also be used to augment the control power and the lift during take-off and landing to reduce runway length[4]. Development and flight testing of thrust vector nozzles for high performance Conventional Take-off and Landing (CTOL) aircraft started in the 1980s. Various research programmes such as F-15-STOL/MTD, F-16 MATV, F-18 HARV and X-31 demonstrated various capabilities of thrust vector control[2,5-7].

There is very little published work in the area of airplane take-off analysis and simulation. The airplane take-off analysis using trim algorithms was proposed by Pashilkar[8] in the early stages of airplane design. In-flight determination of aircraft take-off performance using pilot techniques (control inputs) was studied by Larson *et al*[9]. The take-off distance is very sensitive to pilot techniques and variation in take-off distance of about 20% was reported depending on the rotation speeds. Calvert[10] proposed an optimum procedure for the take-off of AV-8B aircraft with thrust vectoring. Reduction in take-off ground roll using the thrust vector has been reported by many researchers[2,4,11].

The optimal control methodology has been widely used by many researchers[12-16] for analysing airplane manoeuvres. In this work, the airplane take-off problem has been formulated as a multiphase optimal control problem and solved for a twin-engine thrust vector fighter aircraft model F-18/HARV. This paper is organised as follows. In Section 2, the aircraft take-off model is described followed by a description of the aircraft model F-18/HARV in Section 3. Problem formulation and optimal control methodology are presented in Section 4 followed by results and discussions in Section 5 and concluding remarks in Section 6.

2.0 AIRCRAFT TAKE-OFF MODEL

Aircraft take-off can be divided into three distinct phases as shown in Fig. 1, with the duration of each depending on the governing equations and the applicable constraints. Phase I is the ground run where both main landing gear (MLG) and nose landing gear (NLG) are on the ground. Phase II is the rotation phase where the NLG is off the ground and MLG is still on the ground. Phase III consist of the transition and climb where the airplane is airborne.

With take-off primarily being a longitudinal manoeuvre (in the absence of cross-wind), three degree-of-freedom motion (translations along x and z axes, and rotation in pitch θ) constituting longitudinal aircraft dynamics is considered. Equations of motion were modified to incorporate the reaction forces on the main and nose wheel landing gear.

https://doi.org/10.1017/S0001924000008733 Published online by Cambridge University Press

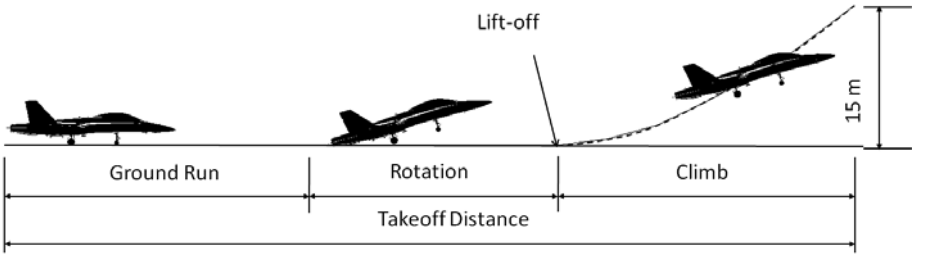


Figure 1. Phases of aircraft take-off.

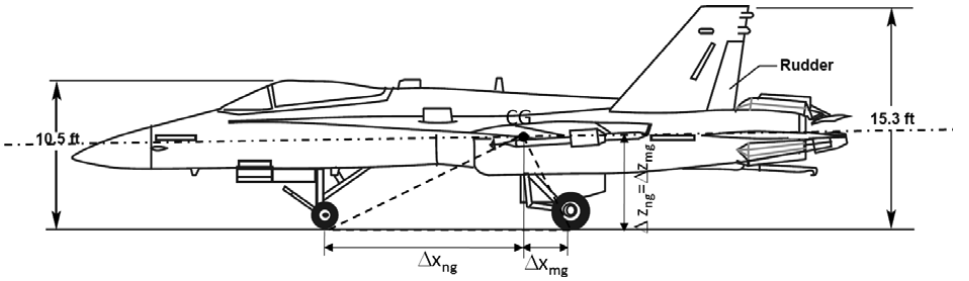


Figure 2. Landing gear geometric parameters.

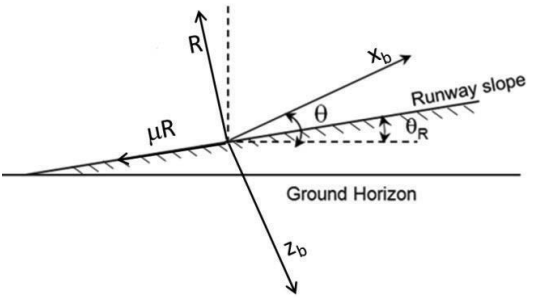


Figure 3. Ground forces and body axis system.

Figure 2 shows the nose and main landing gear positions with respect to the CG of the airplane. Ground forces arise when the landing gear are in contact with the ground. Ground forces consist of the normal reactions (R_{ng} and R_{mg}) and resulting tangential friction forces (as shown in Fig. 3) acting at the nose and main landing gear. Components of these forces along aircraft body axes are as given below.

$$\left.\begin{aligned} F_{Xng} &= R_{ng}\mathrm{Sin}(\theta-\theta_R) - \mu R_{ng}\mathrm{Cos}(\theta-\theta_R) \\ F_{Zng} &= -R_{ng}\mathrm{Cos}(\theta-\theta_R) - \mu R_{ng}\mathrm{Sin}(\theta-\theta_R) \\ F_{Xmg} &= R_{mg}\mathrm{Sin}(\theta-\theta_R) - \mu R_{mg}\mathrm{Cos}(\theta-\theta_R) \\ F_{Zmg} &= -R_{mg}\mathrm{Cos}(\theta-\theta_R) - \mu R_{mg}\mathrm{Sin}(\theta-\theta_R) \end{aligned}\right\} \quad \ldots (1)$$

https://doi.org/10.1017/S0001924000008733 Published online by Cambridge University Press

The runway slope has been taken as zero for the present work. Wind conditions were not considered in this model. The longitudinal airplane equations of motion are:

$$\left.\begin{aligned} \dot{V} &= \frac{1}{m}\left(F_X \operatorname{Cos}\alpha + F_z \operatorname{Sin}\alpha\right) \\ \dot{\alpha} &= q + \frac{1}{mV}\left[F_z \operatorname{Cos}\alpha - F_x \operatorname{Sin}\alpha\right] \\ \dot{q} &= \frac{M}{I_y} \\ \dot{\theta} &= q \\ \dot{x}_E &= V \operatorname{Cos}\gamma \\ \dot{z}_E &= -V \operatorname{Sin}\gamma \end{aligned}\right\} \quad \ldots (2)$$

where,

$$F_X = -D\operatorname{Cos}\alpha + L\operatorname{Sin}\alpha + T_X - mg\operatorname{Sin}\theta + (R_{ng} + R_{mg})\operatorname{Sin}\theta - \mu(R_{ng} + R_{mg})\operatorname{Cos}\theta$$

$$F_Z = -D\operatorname{Sin}\alpha - L\operatorname{Cos}\alpha + T_Z + mg\operatorname{Cos}\theta\operatorname{Cos}\phi - (R_{ng} + R_{mg})\operatorname{Cos}\theta - \mu(R_{ng} + R_{mg})\operatorname{Sin}\theta$$

Conventionally, rotation of the airplane is taken about the MLG ground contact point until the lift-off point and about the CG thereafter. The ambiguity here is that during the rotation phase, the aircraft CG is slightly raised above the ground due to rotation about the MLG whereas equation

$$\dot{z}_E = -V \operatorname{Sin}\gamma$$

predicts the height change as zero, since $\gamma = 0$. In order to avoid such problems, an elegant formulation has been used in this work, in which, the airplane rotation is taken about the CG all through the take-off. The dynamic equation for the height of the airplane CG (z_E) was modified as

$$\dot{z}_E = -V \operatorname{Sin}\gamma - q(\Delta x_{mg}\operatorname{Cos}\theta + \Delta z_{mg}\operatorname{Sin}\theta)$$

while the aircraft is on the ground (i.e. during Phase I and II). This formulation requires constraint equations in Phase I and II of the optimal control problem and the ground reactions R_{ng} and R_{mg} appear as algebraic states. During Phase I, both MLG and NLG are on ground, and in Phase II, only the MLG is on ground. The respective constraint equations are $R_{mg} = R_{ng} = 0$ (height of nose and main wheel tyres are zero) during Phase I and R_{ng} (height of nose wheel tyre is zero) during Phase II. The main and the nose landing gear contact points with reference to CG can be written as,

$$\begin{aligned} z_{mg} &= z_E - \Delta x_{mg}\operatorname{Sin}\theta + \Delta z_{mg}\operatorname{Cos}\theta \\ z_{ng} &= z_E - \Delta x_{ng}\operatorname{Sin}\theta + \Delta z_{ng} \end{aligned} \quad \ldots (3)$$

The aerodynamic data, geometric data and inertia properties of F-18 HARV[17-19] available in public literature have been used in this work. Besides, ground effect on the induced drag is significant during the take-off. It has been taken into account and the F-18/HARV aerodata was modified using the rule[20],

$$\frac{K_g}{K} = \left[24 \cdot 12 * \ln\left(-\frac{h}{b}\right) + 108 \cdot 29\right] \quad \ldots (4)$$

https://doi.org/10.1017/S0001924000008733 Published online by Cambridge University Press

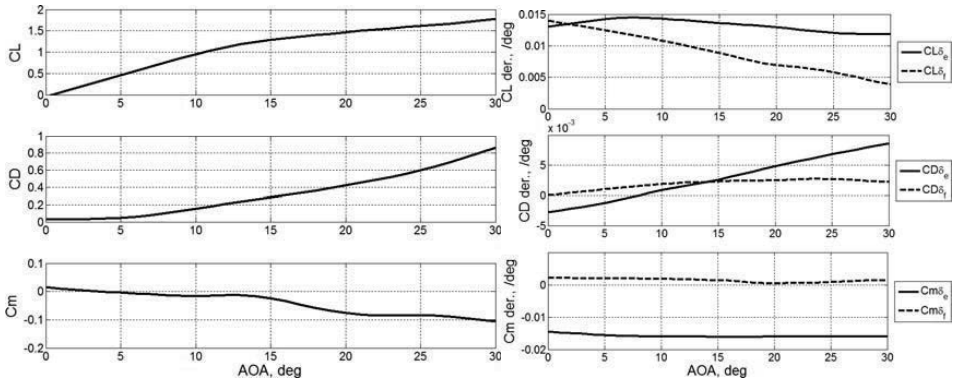


Figure 4. Longitudinal force and moment coefficients and control derivatives.

where, K is induced drag coefficient, K_g is induced drag coefficient with ground effect, h is the height of the wing above ground level and b is the wing span. Further, thrust variation with speed and altitude was calculated from the sea-level static thrust of the engine using the following correlations[21].

$$T = T_{SL}\delta_0\left(1-3\cdot5(\theta_0 - TR)/\theta_0\right) \quad \ldots (5)$$

Where, $\theta_0 = \dfrac{T_{amb}}{288\cdot15}\left(1+\dfrac{\gamma\text{-}1}{2}M^2\right)$, $\delta_0 = \dfrac{P_{amb}}{1\cdot013\times10^5}\left(1+\dfrac{\gamma\text{-}1}{2}M^2\right)^{\dfrac{\gamma}{\gamma-1}}$

T_{amb}, P_{amb} are the ambient temperature and pressure, respectively, M is the flight Mach number, γ is the specific heat ratio, and TR is the throttle ratio. The thrust response from the engine has been modelled as first order dynamics with a time constant of 1·0s.

$$\dot{\eta} + \frac{1}{\tau_p}\eta = \eta_C \quad \ldots (6)$$

where, η is the throttle output, η_c is the throttle command, and τ_p is thrust time constant.

3.0 AIRCRAFT MODEL

The F-18/High-Alpha Research Vehicle (HARV) is a twin-engine airplane with aft-tail configuration. It has all-moving horizontal tail surfaces (stabilator) for pitch control. The aerodynamic data for this aircraft is available in the public domain[17]. The aerodynamic characteristics relevant to the take-off problem are shown in Fig. 4. The data pertaining to flap deflection were obtained from Ref. 18.

The important data of F-18 HARV used in this work are given in Table 1.

The position and rate limits of the controls taken from Ref. 18 are given in Table 2.

The flap deflection in this study was limited to 25°. It would be inappropriate to use larger values of flap deflection as the control derivatives are not available as a function of δ_f.

https://doi.org/10.1017/S0001924000008733 Published online by Cambridge University Press

Table 1
Inertia and geometric data

Weight	16,375kg
Wing reference area	37·16m^2
Mean aerodynamic chord	3·5113m
Reference span	11·4m
Pitch inertia, I_{yy}	238,430kg-m^2
Centre of gravity (CG)	23·8% of MAC

Table 2
Control position and rate limits

Control	Position limits (in deg)	Rate limits (in deg/s)
Stabilator	–4/+10·5	–40/+40
TE flaps	-8/+45	–18/+18
Vector nozzle	–20/+20	–80/+80

3.1 Thrust vector model

The aircraft is powered by two F404-GE-400 afterburning engines. It has externally-mounted nozzle post-exit vanes for thrust vectoring as shown in Fig. 2. This enables both pitch and yaw vectoring of the thrust and a detailed model of vector forces and moments can be found in Ref. 19. The take-off analysis requires only the pitch vectoring model and hence a simple vector nozzle model given below has been used for this work.

The gross thrust produced (F_G) at the nozzle is deflected by the vectoring. Hence, the components of the thrust are

$$\left.\begin{aligned} T_X &= F_G \mathrm{Cos}\delta_{ptv} - m_1 V \mathrm{Cos}\alpha \\ T_Z &= -F_G \mathrm{Sin}\delta_{ptv} - m_1 V \mathrm{Sin}\alpha \end{aligned}\right\} \quad \ldots (7)$$

Where, m_1 is the mass of air entering the engine and δ_{ptv} is the pitch thrust vector angle. The pitching moment produced is

$$M_y = T_z(x_{cg} - x_{noz}) + T_x(z_{eng} - z_{cg}) \quad \ldots (8)$$

The engine gross thrust, $F_G = F_N + m_1 V_1$, where the momentum of inlet air is small at low speeds such as during take-off.

4.0 METHODOLOGY

The aircraft take-off has been formulated as an optimal control problem. The optimal control problem (OCP) minimises the cost function (J) of the form

https://doi.org/10.1017/S0001924000008733 Published online by Cambridge University Press

$$J = \psi(t_f, x(t_f), p) + \int_{t_0}^{t_f} F\left(t, x(t), u(t), p\right) \mathrm{d}t \quad \ldots (9)$$

Subject to state equations: $\dot{x} = f(t, x(t), u(t), p)$,
path constraints: $x_l \le x(t) \le x_u$,
control limits: $u_l \le u(t) \le u_u$,
control rate limits: $\dot{u}_l \le \dot{u}(t) \le \dot{u}_u$,
initial conditions: $x(t_0) = x_0$ and
final conditions: $x(t_f) = x_f$.

For the take-off problem studied here, one of the cost functions is: $J = x_E(t_f)$, i.e. ground distance at final time t_f (take-off distance).

There are two categories of algorithms used to solve the optimal control problems: (a) based on direct methods and (b) based on indirect methods. The direct method replaces the continuous time interval with a grid of discrete points, thus approximating it with a finite-dimensional problem and solved using nonlinear programming (NLP) solvers. The indirect approach preserves the infinite-dimensional character of the problem and uses the theory of optimal control to solve it[22]. The third type of algorithm which takes advantage of both these methods is the pseudo-spectral methods. A Matlab version of the General Pseudo-spectral Optimal Control Software (GPOPS)[23], an open source code has been used in this work. This software is capable of solving the multi-phase problems. In GPOPS the problem is to be defined in the Matlab data structures setup and Matlab functions dae, cost, and link. These functions compute dynamic equations/path constraints, cost function and linkage constraints between phases, respectively. A successful run produces time histories of states, controls, co-states, Hamiltonian, etc. for each of the phases. The take-off problem formulation coded in GPOPS is summarised below.

4.1 Objectives

Objective 1: Minimise take-off distance, i.e. $x^{(3)}_{E,final}$ (distance from brake release to the end of Phase III)
Objective 2: Minimise ground roll distance, i.e. $x^{(2)}_{E,final}$ (distance from brake release to the end of Phase II)
Objective 3: Minimise take-off time, i.e. $t^{(3)}_f$ (time from brake release to the end of Phase III)

State limits: $0 \le V \le 100\text{ms}^{-1}$, $0 \le \alpha \le 13°$, $0{\cdot}3 \le q \le 0{\cdot}3\text{rad/s}$, $-0{\cdot}3 \le q \le 0{\cdot}3\text{rad/s}$, $0 \le \theta \le 20°$, $0 \le x_E \le 1200\text{m}$, $-18 \le z_E \le 0\text{m}$

Control limits: $0 \le \eta \le 1$, $-25° \le \delta_e \le 10{\cdot}5°$, $-20° \le \delta_{ptv} \le 20°$, $-8° \le \delta_f \le 25°$

Control rate limits: $-40°/\text{s} \le \dot{\delta}_e \le 40°/\text{s}$, $-80°/\text{s} \le \dot{\delta}_{ptv} \le 80°/\text{s}$, $-18°/\text{s} \le \dot{\delta}_f \le 18°/\text{s}$

The GPOPS does not support algebraic states and hence R_{ng} and R_{mg} were treated as controls with $z_{ng} = z_{mg} = 0$ (height of nose and main wheel tyres are zero) and $z_{mg} = 0$ (height of main wheel tyre is zero) as path constraints in Phase I and Phase II, respectively. GPOPS also does not allow control rate limits to be specified, therefore, $\dot{\delta}_e$, $\dot{\delta}_{ptv}$ and $\dot{\delta}_f$ have been used as pseudo-controls with appropriate limits. The controls δ_e, δ_{ptv} and δ_f have been used as augmented states. The take-off

https://doi.org/10.1017/S0001924000008733 Published online by Cambridge University Press

problem has been broken into three phases in order to implement the changing constraint equations. The constraint equations change at the instant of nose wheel lift-off and the main wheels lift-off. The model details for each of the three phases are described below.

Phase I
States and controls: $\bar{x} = \{V,\ \alpha,\ q,\ \theta,\ x_E,\ z_E,\ R_{ng},\ \eta,\ \delta_e,\ \delta_{ptv},\ \delta_f\}$, $\bar{u} = \{\eta_c,\ \dot{\delta}_e,\ \dot{\delta}_{ptv},\ \dot{\delta}_f,\ \dot{R}_{ng},\ R_{mg}\}$
Path constraints: $R_{ng} = R_{ng} = 0$
Initial conditions: $V = 0, X_E = 0, z_E = -1{\cdot}9\text{m}$
Final conditions: $R_{ng} = 0$

Phase II
States and controls: $\bar{x} = \{V,\ \alpha,\ q,\ \theta,\ x_E,\ z_E,\ R_{mg},\ \eta,\ \delta_e,\ \delta_{ptv},\ \delta_f\}$,
Path constraints: $z_{mg} = 0,\ 0 \le \alpha \le 13°$
Linkage constraints:
Final conditions: $R_{mg} = 0$

Phase III
States and controls: $\bar{x} = \{V,\ \alpha,\ q,\ \theta,\ x_E,\ z_E,\ R_{mg},\ \eta,\ \delta_e,\ \delta_{ptv},\ \delta_f\}$, $\bar{u} = \{\eta_c, \dot{\delta}_e, \dot{\delta}_{ptv}, \dot{\delta}_f, \dot{R}_{mg}\}$
Path constraints: $0 \le \alpha \le 16°,\ 0 \le \theta \le 20°$
Linkage constraints: $x^{(2)}_{1\ldots6,\text{initial}} = x^{(1)}_{1\ldots6,\text{final}}$
Final conditions: $z_E = -16{\cdot}9,\ q = 0,\ \gamma = \theta - \alpha > 4°$

In the climb phase of the take-off, the obstacle height of 15m was taken, which leads to a vertical travel of the CG (z_E) from –1·9m to –16·9m.

The wheel reactions R_{ng} and R_{mg} should reach zero at the end of Phase I and Phase II, respectively. These end conditions can be specified only for the state variables and not for the controls. To overcome this difficulty, $\dot{R}_{ng}$ and $\dot{R}_{mg}$ have been used as controls and R_{ng} and R_{mg} were made augmented state variables respectively in Phase I and Phase II.

5.0 RESULTS AND DISCUSSIONS

The optimal control solution for the take-off of the F-18/HARV airplane has been computed using GPOPS with four different control strategies. The computations were performed using combinations of different pitch control effectors, using: only (1) stabilator, (2) stabilator and flaps, (3) stabilator and thrust vector nozzle, and (4) stabilator, thrust vector nozzle and flaps. These computations were carried out to understand the extent of benefit possible by the use of thrust vector nozzle in combination with the other controls in reducing the take-off distance.

The objectives of optimisation in take-off of an airplane are reduction of take-off distance and ground roll distance. The take-off distance includes the climb distance of the climb phase where the aircraft reaches 15m obstacle height above the ground after lift-off. The ground roll distance does not include the climb phase; it is the runway distance covered from the time of brake release to lift-off (consisting of Phases I and II alone). Reducing the ground roll distance is a more relevant objective when the airplane is required to take-off from the available length of a damaged runway. The third objective which was considered in this study is the minimisation of take-off time. The cost function in each case is different as listed in the previous section. The results are summarised in Tables 3 to 5, respectively, for minimum take-off distance, minimum ground roll distance and minimum time to take-off.

https://doi.org/10.1017/S0001924000008733 Published online by Cambridge University Press

Table 3
Minimum distance take-off results

Parameter	Case (1)	(2)	(3)	(4)
Rotation speed, ms^{-1}	62·1	54·0	17·0	17·0
Lift-off speed, ms^{-1}	76·4	68·2	68·7	62·6
Distance in ground roll, m	404·1	320·2	320·0	266·6
Distance in climb, m	233·2	219·1	267·5	243·0
Total distance, m	637·3	539·3	587·5	509·3
Total time, s	13·17	12·12	12·66	11·81

Table 4
Minimum ground roll take-off results

Parameter	Case (1)	(2)	(3)	(4)
Rotation speed, ms^{-1}	61·3	53·7	17·0	17·0
Lift-off speed, ms^{-1}	74·3	67·7	63·3	57·4
Distance in ground roll, m	401·2	314·7	272·8	222·8

Table 5
Minimum time to take-off results

Parameter	Case (1)	(2)	(3)	(4)
Rotation speed, ms^{-1}	62·2	54·8	60·8	55·5
Lift-off speed, ms^{-1}	76·2	68·2	69·2	63·1
Distance in ground roll, m	402·0	319·6	324·2	268·7
Distance in climb, m	235·9	219·5	263·5	239·1
Total distance, m	637·9	539·1	587·7	507·8
Total time, s	13·17	12·11	12·63	11·75

5.1 Minimum distance to take-off

Results of all the four cases with minimising take-off distance as the objective function is summarised in Table 3. The take-off distance by using only the stabilator control (Case (1)) is 637·0m. Use of flaps or thrust vector nozzle reduces the take-off distance substantially (Case (2) and (3)). A further reduction in take-off distance is achieved by using all three controls (Case (4)) together. The reduction in take-off distance with the use of thrust vector nozzle in combination with flaps was found to be about 6% and 20% respectively as compared to Case (2) and Case (1). The major benefit of using thrust vector nozzle is found to be in the reduction of ground roll distance where it reduces from 320·2m to 266·6m (reduction of 17%).

Time histories of states and controls of the optimal take-off are shown in Fig. 5 for Case (2) where stabilator and flaps were used for pitch control.

Figure 5(a) shows the time history of states along with the nose and main wheel ground reactions (R_n and R_m). The nose wheel reaction starts reducing at 6s when the stabilator is deflected trailing-edge up and reaches zero when nose wheel lifts-off at the end of Phase I. As seen from the Fig. 5(b), the flaps are deflected to maximum trailing-edge down position almost all through the take-off. The stabilator is also at the maximum trailing-edge down position during ground

https://doi.org/10.1017/S0001924000008733 Published online by Cambridge University Press

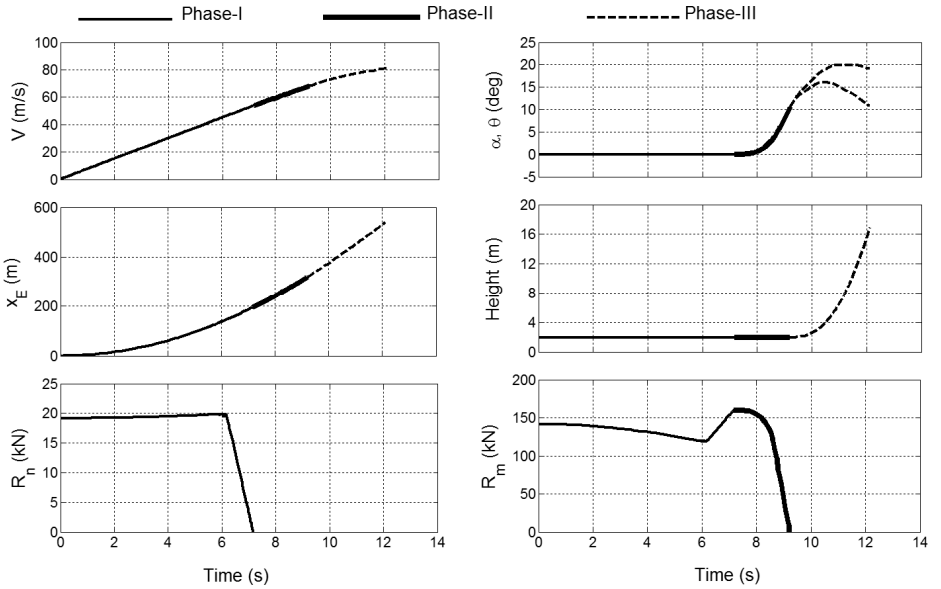


Figure 5(a). Case (2) Time history of states.

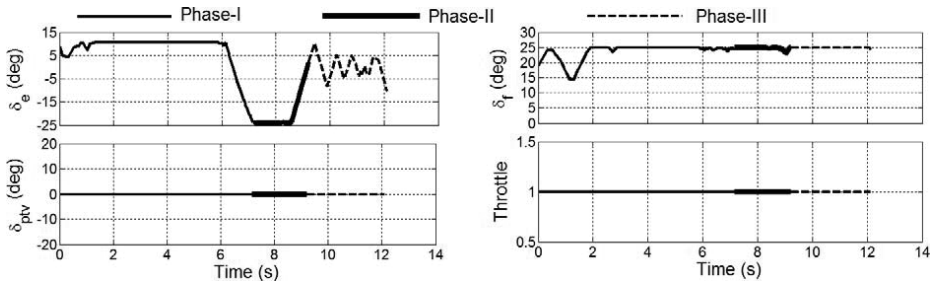


Figure 5(b). Case (2) Time history of controls.

roll and is deflected to maximum trailing-edge up position to rotate the airplane to take-off AoA. Before the AoA reaches the limiting AoA (scrape angle limit), the stabilator is deflected trailing-edge down to augment lift. However, the AoA continues to increase to take-off AoA due to inertial moment and the airplane lifts off the ground which is indicated by main gear reaction becoming zero. The engine throttle is at its maximum throughout the take-off as expected, to provide the maximum acceleration to the airplane. The pitch attitude has reached its limiting value of 20° specified for the climb phase as shown in the figure. The lower curve (AoA) decreases during the climb as the speed increases and the climb angle ($\theta - \alpha$) is about 9° which is higher than the lower limit of 4° specified.

https://doi.org/10.1017/S0001924000008733 Published online by Cambridge University Press

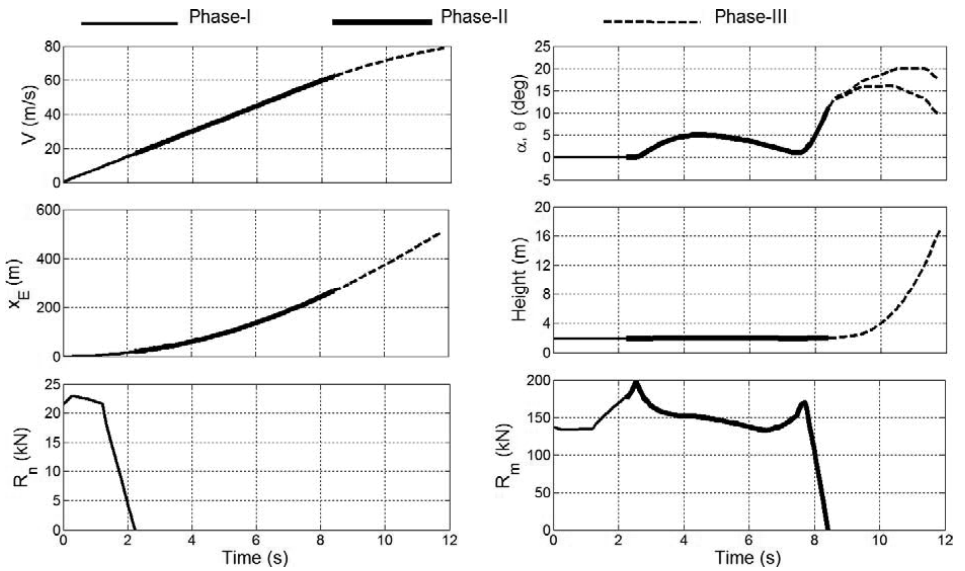


Figure 6(a). Case (4) Time history of states.

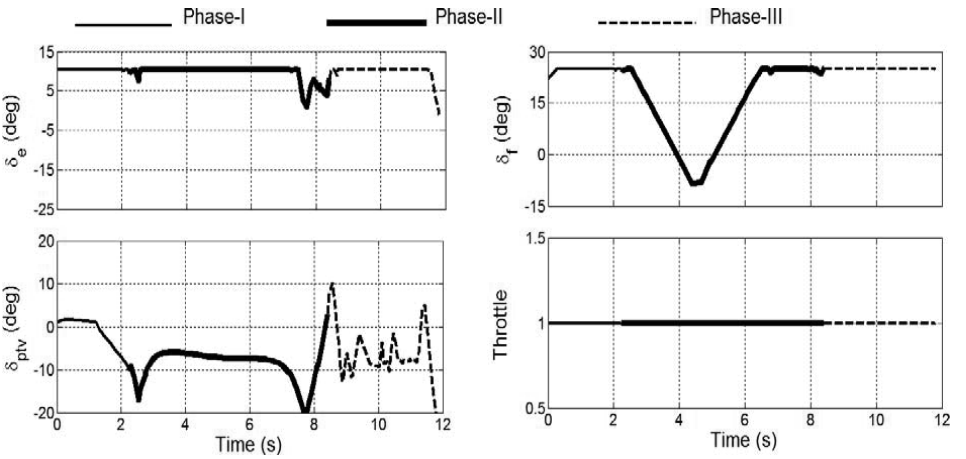


Figure 6(b). Case (4) Time history of controls.

The results of computations for Case (4), i.e. using all three pitch control effectors stabilator, flaps and thrust vector nozzle are shown in Fig. 6.

The reduction in take-off distance (over Case (2)) was achieved with thrust vector control. The major difference in the control strategy in this case is the early rotation; the rotation is initiated at a speed of 17·0ms^{-1}. Lift-off is initiated by deflecting the nozzles upwards. Pitch control power of the thrust vector is sufficiently high to rotate the aircraft even at zero speed. The rotation was initiated at a speed of 17·0ms^{-1}because that was the minimum limit specified for the speed at the end of the Phase I. The main reason for lower ground roll distance is due to lowering of the lift-off speed from 68·2ms^{-1} (Case (2)) to 62·6ms^{-1}. This was possible due to the enhancement in lift by maximum downward deflection of both flaps and stabilator.

https://doi.org/10.1017/S0001924000008733 Published online by Cambridge University Press

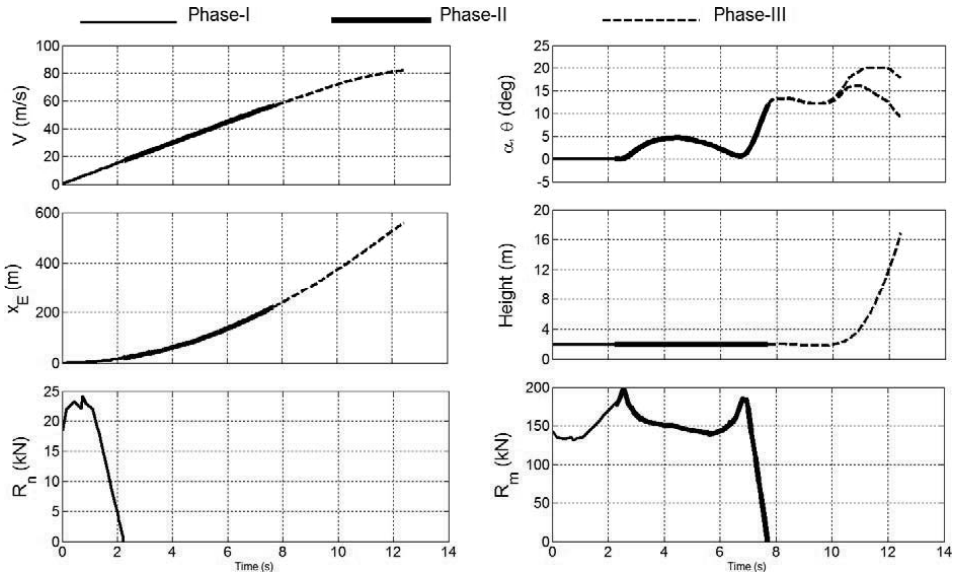


Figure 7(a). Minimum ground roll take-off: States.

It is interesting to note that the thrust vector nozzle deflection does not add to the lift, in fact, it reduces the lift. But, the thrust vector nozzle is useful for trimming the pitch-down moment due to the trailing-edge down deflection of the flaps and stabilator. However, at the time of lift-off the thrust vector nozzle is deflected downwards momentarily to enhance lift for low speed lift-off. The throttle is at the maximum thrust setting throughout the take-off as expected. The other important observation is that the nose rotation takes place in two steps; initially the nose is rotated to about 5° AoA and in the second step it is rotated to take-off AoA at lift-off. This is the optimum control strategy from the drag point of view; the minimum drag provides maximum acceleration to reach lift-off speed. At zero AoA the induced drag is minimum, but the friction drag on the wheels is maximum due to higher reaction forces; whereas at higher AoA, the ground reaction is reduced due to the lift but the induced drag is higher. Hence there is an intermediate AoA at which the net drag is minimum and that is the reason why the airplane is held at an intermediate AoA until it accelerates to the lift-off speed.

5.2 Minimum ground roll take-off

Results of the analysis with minimising the ground roll distance as the objective are shown in Fig. 7 for Case (4). The ground roll distance is reduced from 266·6m to 222·8m as a result of lower lift-off speed. There are few subtle differences between Figs 6 and 7. The AoA at the time of lift-off has increased to 12·0° from 11·2°. The downward nozzle deflection is 7·5° against 1·5°. Both these factors help in early lift-off. Another important difference to notice is the airplane flight path after lift-off. In the case of minimum ground roll take-off, the airplane does not climb for about 2s after lift-off and starts climbing only thereafter; the airplane gains speed and then climbs. This results in higher distance to climb to 15m obstacle height after lift-off. In fact the distance covered in Phase III does not affect the cost function. The distance covered in this phase was found to be the

https://doi.org/10.1017/S0001924000008733 Published online by Cambridge University Press

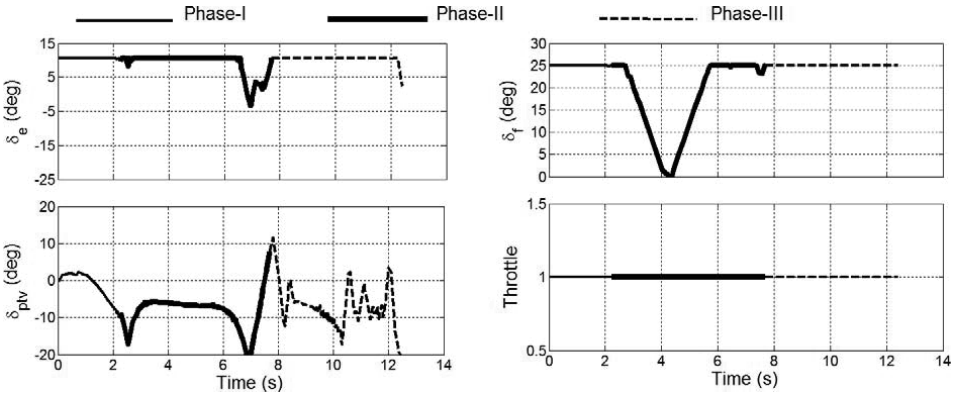


Figure 7(b). Minimum ground roll take-off: controls.

Table 6
Results for simplified control strategy

Parameter	Objective function		
	Min TO distance	Min ground roll	Min time
Rotation speed, ms^{-1}	18·3	17·0	54·4
Lift-off speed, ms^{-1}	62·6	57·6	63·1
Distance in ground roll, m	265·9	226·2	268·9
Distance in climb, m	244·3	169·7	239·7
Total distance, m	510·2	544·5	508·6
Total time, s	11·81	12·24	11·76

upper limit specified for the state variable x_E in this phase. Hence, the corresponding data for the climb phase is irrelevant and hence they were not shown in Table 4.

5.3 Minimum time take-off

The computations were also carried out with minimisation of take-off time as the cost function and the results were found to be almost same as that obtained with minimisation of take-off distance as the cost function as shown in Table 3 and Table 5.

5.4 Simplified control strategy

From the above results discussed it is clear that there is a significant benefit of using thrust vector nozzle for the take-off and also we must use all the available pitch control effectors to get the best results. However, it is not practical to use all these controls simultaneously by the pilot and some kind of automatic scheduling would be necessary. Interestingly, a further study of the control history leads to a simplified control schedule which results in a performance which is close to Case (4). In the simplified control scheme, the stabilator and the flaps were fixed at their maximum trailing-edge down position and an optimum thrust vector control schedule was computed. The results are presented in Table 6. The time history of states and controls are shown in Fig. 8.

https://doi.org/10.1017/S0001924000008733 Published online by Cambridge University Press

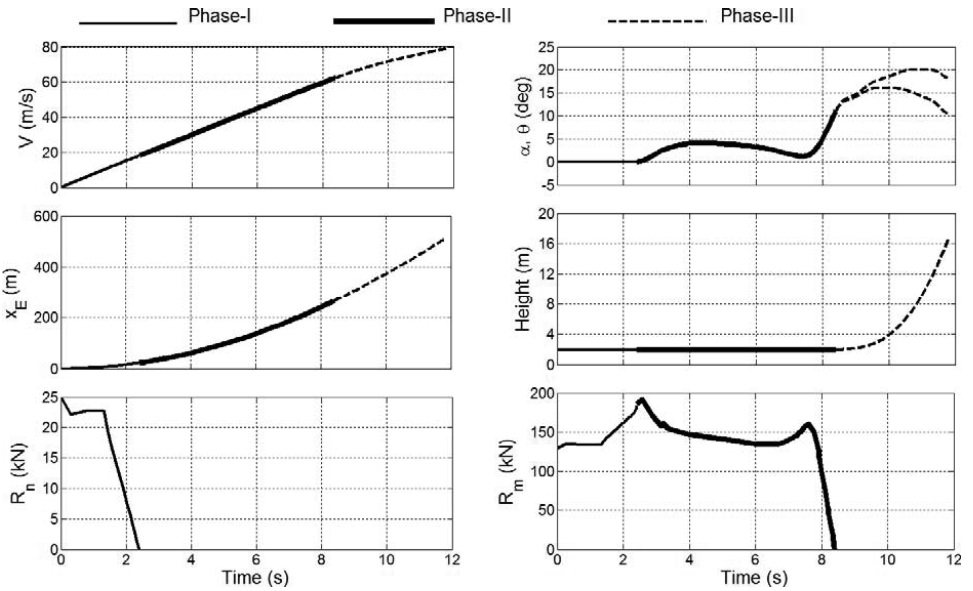


Figure 8(a). Simplified control strategy: states.

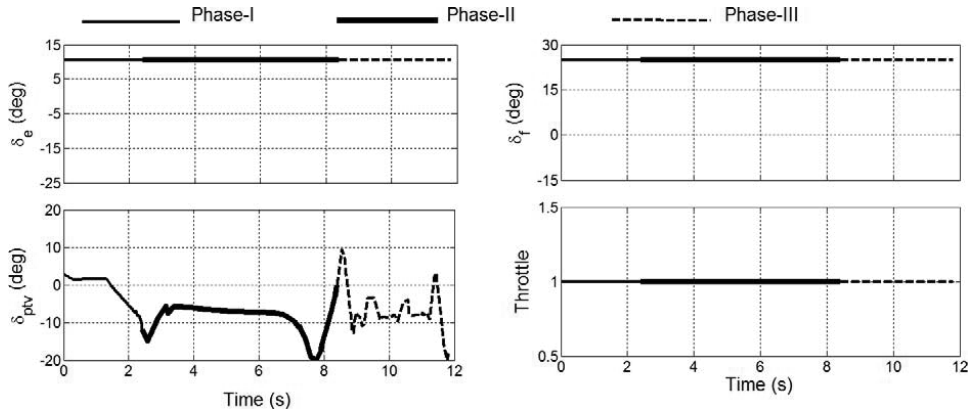


Figure 8(a). Simplified control strategy: controls.

The results show that the simplified control strategy is as good as the complex control strategy where all three control (stabilator, flaps and vector nozzle) deflections have to be optimised. Hence, this simplified control may be used by the pilot to manually execute the take-off. By fixing the stabilator and flaps to their maximum trailing-edge down position, the nozzle deflection schedule has changed only marginally as shown in Fig. 9.

5.5 Tail scrape constraint

As mentioned above, the take-off AoA is limited to 13° to avoid the tail touching the runway. However, after the lift-off, when the airplane climbs, the tail scrape constraint is no longer effective thus allowing pitch attitude and the AoA to change freely. When optimal control computations were

https://doi.org/10.1017/S0001924000008733 Published online by Cambridge University Press

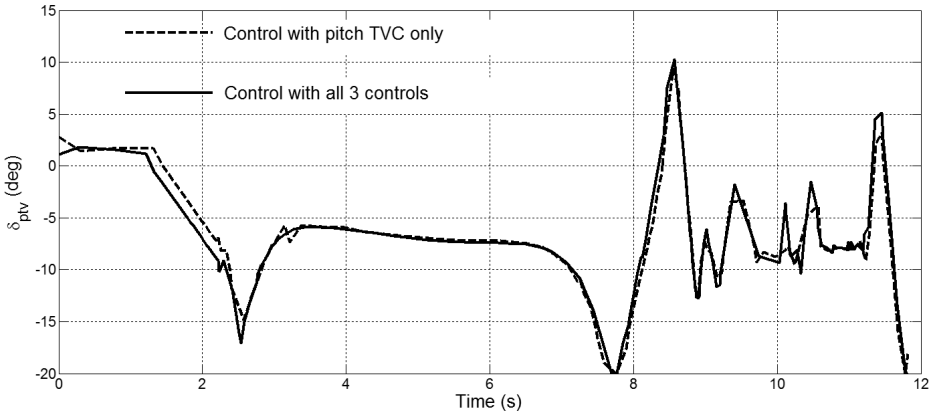


Figure 9. Nozzle deflection comparison.

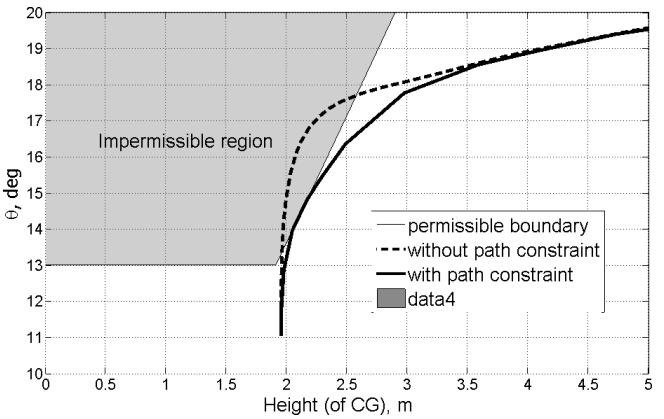


Figure 10. Constraint to avoid tailscrape.

carried out relaxing this constraint, it was found that the airplane rotates to higher pitch attitude before climbing to sufficient height immediately after lift-off. To overcome this problem, a path constraint was imposed on the optimisation.

The path constraint was formulated as $\theta \le \mathrm{Sin}^{-1}\left(\frac{z}{z_0}\mathrm{Sin}13^0\right)$ which ensures that the tail does not touch the ground after the lift-off. The optimum pitch angle computed with and without this path constraint for Case (1) problem is shown in Fig. 10. The shaded region is the impermissible region where the tail would hit the runway. It was found that the take-off distance is increased by about 12m by imposing this constraint.

5.6 Effect of early rotation

When thrust vector control is used for take-off, the optimum control demands the rotation be initiated at very low speed. Even though the thrust vector control power is capable of rotating the airplane at zero speed, a minimum speed is required for the handling of the airplane on ground and

https://doi.org/10.1017/S0001924000008733 Published online by Cambridge University Press

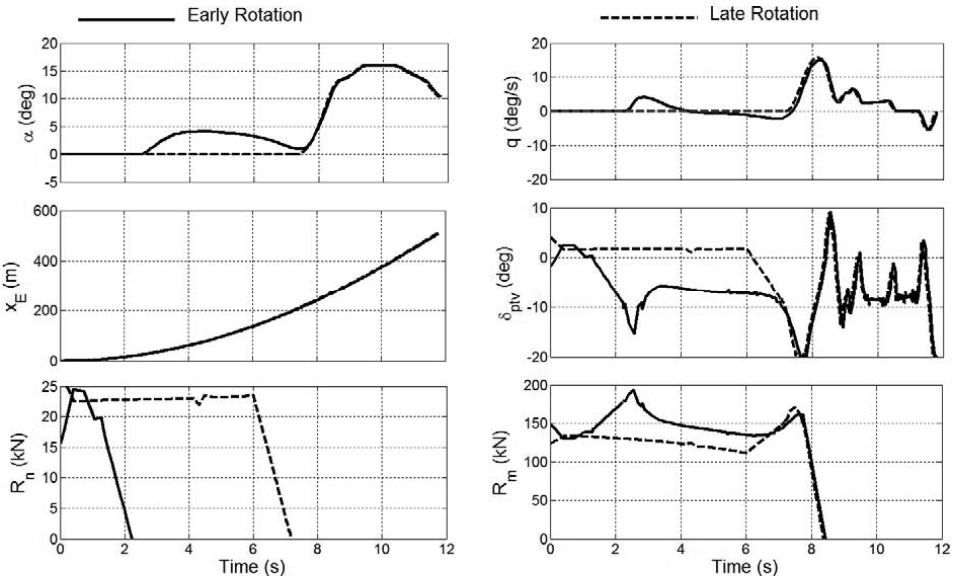


Figure 11. Effect of early rotation.

hence a minimum speed of 17·0ms^{-1} has been specified for the computations. The computations with thrust vector nozzle shows that the early rotation is optimum for the reduction of take-off distance. However, it does not show what would be the penalty if the rotation is delayed until the aircraft accelerates to a speed sufficient for rotation with aerodynamic control only. To understand this, computations was repeated by forcing the rotation speed to a higher value. A comparison of results is shown in Fig. 11. Even though there are major differences in the way the take-off is executed between the early and late rotation cases, there is negligible difference in the take-off distance. Hence it is concluded that there is no significant benefit in rotating the nose early even if the control power is available through thrust vectoring.

5.7 Effect of aerocraft centre of gravity

The effect of CG position on the optimal take-off distance was analysed by varying the CG position from –5% (aft CG) to +5% (forward CG) of the mean aerodynamic chord (MAC). Figure 12 shows the variation of take-off distance with the CG movement. The forward CG movement increases the take-off distance significantly. The time history of take-off parameters are shown in Fig. 13 for the two extreme CG locations. In the case of forward CG location (+5%), the nose gear reaction is much higher and hence the airplane requires much higher pitch-up moment to rotate the aircraft. Both flap and nozzle are deflected up relative to the rearward CG case. This causes lower lift and hence the lift-off speed is increased resulting in increase of take-off distance.

https://doi.org/10.1017/S0001924000008733 Published online by Cambridge University Press

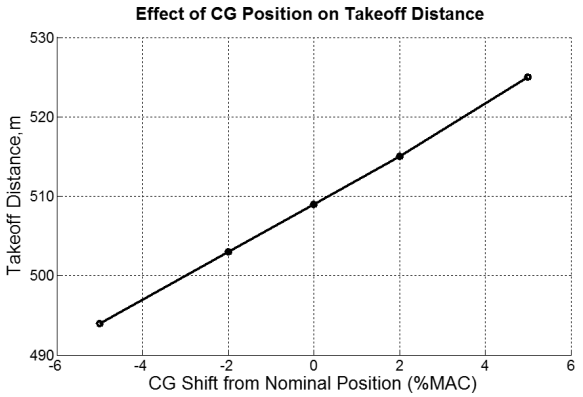


Figure 12. Effect of CG location on take-off.

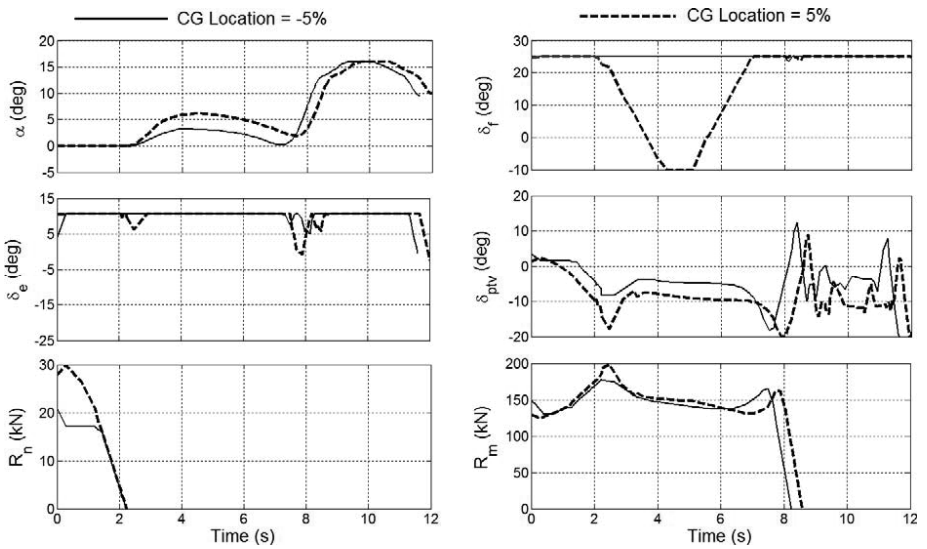


Figure 13. Take-off time histories for extreme CG locations.

6.0 CONCLUSIONS

Optimal control methodology can be applied to the airplane take-off problem to arrive at the control strategies which minimise the take-off distance and take-off ground roll. In particular, it is very useful when there are many pitch control effectors such as elevator, flaps, canard and thrust vector nozzle. The role of the each control is strongly dependent on the presence of other controls available. Use of thrust vectoring control considerably reduces both the take-off distance and ground roll distance. A reduction of about 6% in take-off distance and about 29% in ground roll distance were obtained for the configuration studied with the use of thrust vectoring. Hence, the thrust vectoring is more beneficial in decreasing the ground roll distance, which can be useful when the airplane needs to operate from the available length of a damaged runway.

https://doi.org/10.1017/S0001924000008733 Published online by Cambridge University Press

Thrust vector control possesses large pitch control power to rotate the nose at lower speed. This could be of great help to a configuration which has lower pitch control power or the take-off configuration when the CG is at most forward location, but with a lower lift-off speed (low wing loading). However, for the configuration analysed in this work, early rotation had negligible benefit in reducing take-off distance. Moreover, rotating the nose at very low speeds poses handling quality issues and is not practical for a manned aircraft.

Reduction in take-off distance is effected by the reduction in lift-off speed. The reduction in lift-off speed is strongly dependent on the lift augmentation by optimum use of available controls. However, the thrust vector nozzle is not deflected downward to augment lift for the configuration studied. The nozzle is actually deflected up, during rotation and trimming during climb. The lift is augmented by the flaps and stabilator, and the nozzle deflection is used for trimming the pitching moment. The thrust vectoring here actually contributes negative lift.

The control schedules of stabilator, flaps and thrust vector nozzle computed for optimal take-off would be too complex to be executed by a human pilot. A simplified control schedule was derived based on the optimal control computations, where the flap was fixed at +25°, stabilator was fixed at +10·5° and controlled using thrust vector nozzle only. It was shown that this simplified control gives a performance which is close to the minimum take-off distance obtained using all the controls.

REFERENCES

1. IKAA, D. Thrust vectoring nozzle for modern military aircraft, 2000, NATO R&T Organizations Symposium on Active Control Technology for Enhanced Performance, 8-11 May 2000, Braunschweig, Germany.
2. ROSS, H. and HUBER, P. Application of thrust vectoring to future aircraft design, September 1995, AGARD-CP-572.
3. ALCORN, C.W., CROOM, M.A., FRANCIS, M.S. and ROSS. H. The X-31 aircraft: Advances in aircraft agility and performance, *Prog Aerospace Sci*, 1996, **32**, pp 277-413.
4. BAOKAI, Z. Preliminary study on effects of thrust vectoring, 1995, NAIC-ID (RS)T-0212-95.
5. ALBION, H., BOWERS, J.W.P. Thrust vectoring on the NASA F-18 high alpha research vehicle, 1996, NASA-TM-4771.
6. O'ROURKE. M.J., RALSTON, J.N. and BELL. J.W. PC-based simulation of the F-16/MATV, 1997, AIAA-3728.
7. SMOLKA, J.W., WALKER, L.A., JOHNSON, G.H. and SCHKOLNIK, G.S. F-15 ACTIVE flight research program, NASA Dryden Flight Research Center, http://www.nasa.gov/centers/dryden/pdf/89247main_setp_d6.pdf
8. PASHILKAR, A.A. Algorithms for aircraft trim analysis on ground, 1996, AIAA-3505-CP.
9. LARSON, T.J. and SCHWEIKHARD. W.G. A simplified flight test method for determining aircraft take-off performance that includes the effect of pilot techniques, 1974, NASA TN D-7603.
10. CALVERT, J.F. Method for the determination and optimization of vectored thrust take-off performance, January 1988, Technical Memo, Strike Aircraft Test Directorate, Naval Air Test Center, Patuxent River, Maryland, USA.
11. CARTER, B.R. Time Optimization of High Performance Combat Manoeuvres, 2005, MSc thesis, Naval Postgraduate School.
12. FAN, Y., LUTZE, F. and CLIFF, E. Time-optimal lateral manoeuvres of an aircraft, *J Guidance, Control and Dynamics*, September-October1995, **18**, (5), pp 1106 -1112.
13. TAKANO, H., WADA, H., YAMASAKI, T. and BABA, Y. Optimal vertical manoeuvres of the aircraft with thrust vectoring in the rigid body model, 2007, International Conference on Control, Automation and Systems, 17-20 October 2007, Seoul, South Korea.
14. SATYANARAYANA, G., PRASAD, U.R. and SARMA, I.G. Optimal control for the rolling pullout manoeuvre of a modern fighter aircraft, 1975, IEEE Conference on Decision and Control, Houston, December 1975, Texas, USA.
15. BUELL, G. and LEONDES, C.T. Optimal aircraft go-around and flare manoeuvre, *IEEE Transactions on Aerospace and Electronic Systems*, March 1973, **9**, (2).
16. ONG, S.Y., PIERSON, B.L. and LIN, C.F. Optimal evasive aircraft manoeuvres against a surface-to-air missile, IEEE Regional Conference on Aerospace Control Systems, 25-27 May 1993.

https://doi.org/10.1017/S0001924000008733 Published online by Cambridge University Press

17. http://www.nasa.gov/centers/dryden/history/pastprojects/HARV/Work/NASA2/nasa2.html
18. ILIFF, K.W. and WANG, K.C. Flight-determined subsonic longitudinal stability and control derivatives of the F-18 high angle of attack research vehicle (HARV) with thrust vectoring, 1997, NASA-TP-206539.
19. BOWERS, A.H. and PAHLE, J.W. Thrust vectoring on the NASA F-18 high alpha research vehicle, 1996, NASA-TM-4771.
20. Take-off & Landing, http://allstar.fiu.edu/aero/to%26land.htm.
21. MATTINGLY, J.D. *Aircraft Engine Design*, Second edition, 2002, AIAA Educational Series.
22. SUBCHAN, S. and ZBIKOWSKI, R. *Computational Optimal Control — Tools and Practice*, 2009, John Wiley & Sons.
23. RAO, A.V. User's Manual for GPOPS Version 4.x: A MATLAB software for solving multiple-phase optimal control problems using hp-adaptive pseudospectral methods, 2011.

https://doi.org/10.1017/S0001924000008733 Published online by Cambridge University Press